Investigation of Structural, SEM, TEM and Dielectric Properties of BaTiO₃ nanoparticles

Suresh Sagadevan[1], Jiban Podder[2]

[1] *Department of Physics, AMET University, Kanathur, Chennai 603112, India*
[2] *Department of Chemical and Biological Engineering, University of Saskatchewan, Saskatoon, SK S7N 5A9, Canada*

BaTiO₃ nanoparticles were prepared by solvothermal method. The X-ray diffraction (XRD) analysis was used to study the structure and crystallite size of BaTiO₃ nanoparticles. The morphology and the size of the BaTiO₃ nanoparticles were characterized using scanning and transmission electron microscopy (SEM and TEM). The optical properties were studied using the UV-Visible spectrum in the wavelength range of 300-800 nm. The dielectric properties of BaTiO₃ nanoparticles were studied for different frequencies and different temperatures. The AC electrical conductivity study revealed that the conduction depended both on the frequency and the temperature.

Keywords: BaTiO₃ nanoparticles, XRD, UV analysis, Dielectric studies and AC conductivity.

PACS numbers: 61.46.Df, 68.37.Lp

1. INTRODUCTION

Barium titanate (BaTiO₃) is extensively used in electronic devices in the technological ceramic industry because of its ferroelectric, thermoelectric, and piezoelectric properties when it assumes the tetragonal structure [1]. As such, it can be broadly used in capacitors, positive temperature coefficient resistors, dynamic random access memories, electromechanics, and non-linear optics [2, 3]. For the existence of the size effect of ferroelectricity and the potential application of bottom-up assembled novel nanostructures, the synthesis of ultrafine BaTiO₃ nanoparticles is theoretically and technologically important [4].Very high value of dielectric constant of BaTiO₃ [5, 6] makes it a particularly attractive material from which capacitors, condensers and other electronic components can be fabricated [7, 8]. BaTiO₃ with a perovskite structure is a strong dielectric material, which has far reaching applications in the electronics industry for transducers, actuators, and high-k dielectrics [9, 10]. With the growth of material science and technology, BaTiO₃ powders are expected to have characteristics of fine grain, few agglomerations and uniform composition, over and above higher dielectric constant. As BaTiO₃ offers the above characteristics, the synthetic methods of BaTiO₃ nanopowders have attracted extensive consideration. There are several reports available in the literature on the preparation of well crystalline BaTiO₃ by different methods, such as homogeneous co-precipitation [11, 12], hydrothermal synthesis [13, 14], the sol-gel method [15], etc. The prepared BaTiO₃ nanoparticles were characterized by powder X-ray diffraction analysis, scanning electron microscopy (SEM), transmission electron microscopy (TEM), UV-analysis and electrical studies.

2. EXPERIMENTAL METHODS

Ba and Ti alkoxide precursor [BaTi(OR)₆] solutions were prepared by dissolving equimolar amounts of Barium metal and Titanium isopropoxide in a mixed solvent of anhydrous Benzene and anhydrous Isopropanol. The resulting mixture was mixed at 45 °C with a mag-

netic stirrer until the Barium metal was completely dissolved. The synthesis process of precursor solutions was performed under a nitrogen atmosphere. The mixture was stirred with a magnetic stirrer for 3 hours. The sealed autoclave was heated to 250 °C for 72 hours. After cooling to room temperature, the resultant precipitate was centrifuged and dried at 50 °C for 24 hours in an oven. The XRD pattern of the BaTiO₃ nanoparticles was recorded by using a powder X-ray diffractometer (Schimadzu model: XRD 6000 using CuKα with a diffraction angle between 20° and 80°. The crystallite size was determined from the broadenings of corresponding X-ray spectral peaks by using Debye Scherrer's formula. Scanning Electron Microscopy (SEM) was carried out on JEOL, JSM- 67001. The optical absorption spectrum of the BaTiO₃ nanoparticles was taken by using the VARIAN CARY MODEL 5000 spectrophotometer in the wavelength range of 300-800 nm. The dielectric properties of the BaTiO₃ nanoparticles were analyzed using a HIOKI 3532-50 LCR HITESTER over the frequency range 50 Hz-5 MHz.

3. RESULTS AND DISCUSSION

3.1 X-ray Diffraction Analysis

The phase composition and the structure of the nanoparticles were studied by X-ray diffraction analysis. Fig. 1 shows X-ray diffraction patterns of BaTiO₃ nanoparticles. The broadening of the diffraction peaks due to the size effect hinders us in estimating the crystal structure. FWHM of peaks corresponding to multiple planes is broader than that for a single plane (111), which implies that a tetragonal phase exists in the BaTiO₃ nanoparticles. BaTiO₃ nanoparticles synthesized in this study have a wide distribution of particle size, which means that the prepared nanoparticles have a cubic phase. The crystallite size was determined from the broadenings of corresponding X-ray spectral peaks by using Debye Scherrer's formula. The average nano-crystalline size (*D*) was calculated using the Debye-Scherrer formula,

$$D = 0.9\lambda / \beta \cos\theta, \tag{1}$$

where λ is the X-ray wavelength, θ is the Bragg diffraction angle, and β is the FWHM of the XRD peak appearing at the diffraction angle θ. The average crystalline size was calculated from X-ray line broadening peak and Debye-Scherrer equation and it was found to be about 22 nm.
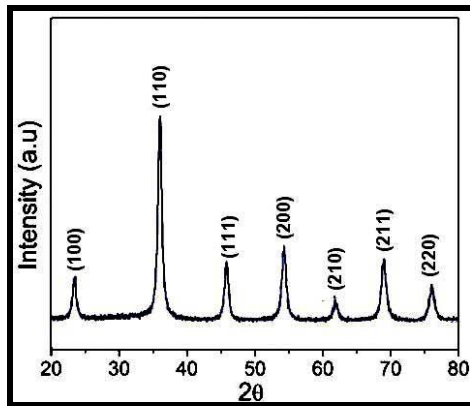

Fig. 1 – XRD spectrum of BaTiO3 nanoparticles

3.2 Scanning Electron Microscopy (SEM)

The morphology of the nanocrystallites is shown in Fig. 2. The SEM pictures clearly show randomly distributed grains with smaller size and the homogeneous spherical shaped particles. The image reveals that the average crystalline size is around 18 nm.
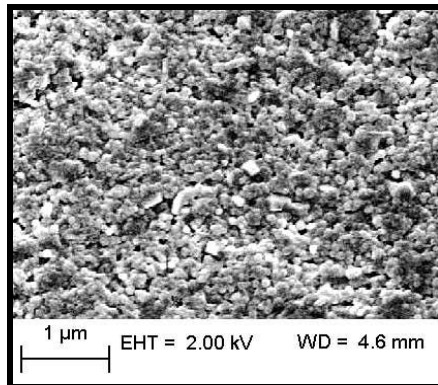

Fig. 2 – SEM image of BaTiO3 nanoparticles

3.3 Transmission Electron Microscopy (TEM)

TEM is commonly used for imaging and analytical characterization of the nanoparticles to assess the shape, size, and morphology. TEM image of the as-prepared spherical shaped BaTiO3 nanoparticles is shown in Fig. 3. In addition to the individual particles, some aggregates are also present. The particle sizes are measured in the range of 25 to 30 nm.

3.4 Optical Studies

The optical absorption spectrum of $BaTiO_3$ nanoparticles was recorded in the wavelength region 300-800 nm and it is shown in Fig. 4. It is important to note that $BaTiO_3$ nanoparticles are very much transparent in the visible region. The dependence of optical absorption coefficient on photon energy helps to analyze the band structure and the type of transition of electrons. The
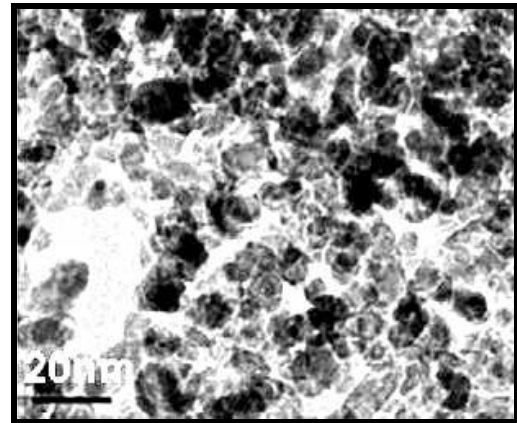

Fig. 3 – TEM image of BaTiO3 nanoparticles

optical absorption coefficient (α) was calculated from transmittance using the following relation

$$\alpha = \frac{1}{d}\log\left(\frac{1}{T}\right) \qquad (2)$$

where T is the transmittance and d is the thickness of the nanoparticle. Determination of optical band gap is based on the photon induced electronic transition between conduction band and valance band. As a direct band gap material, the nanoparticles under study has an absorption coefficient (α) obeying the following relation for high photon energies ($h\nu$) and can be expressed as

$$\alpha = \frac{A(h\nu - E_g)^{1/2}}{h\nu} \qquad (3)$$

where E_g is the band gap of the $BaTiO_3$ nanoparticles and A is a constant. A plot of variation of $(\alpha h\nu)^2$ versus $h\nu$ is shown in Fig. 5. Using Tauc's plot, the energy gap (E_g) was calculated to be 3.40 eV. This was used to find out the nature of transition in the material.
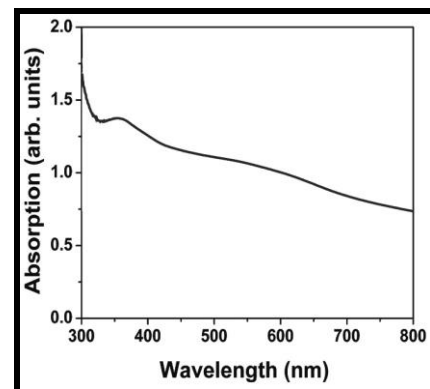

Fig. 4 – UV-Visible absorption spectrum of $BaTiO_3$ nanoparticles

3.5 Dielectric Studies

The dielectric constant was analyzed as a function of the frequency at different temperatures as shown in Fig. 6, while the corresponding dielectric loss is shown in Fig. 7. The dielectric constant is evaluated using the relation,

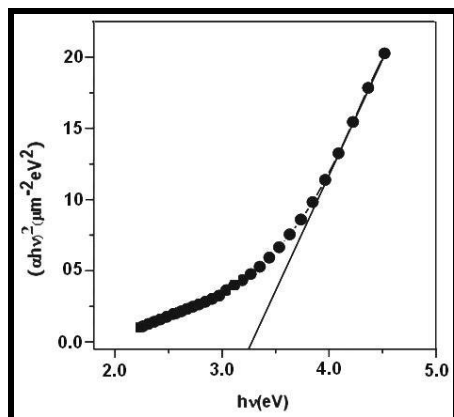$$\varepsilon_r = Cd/\varepsilon_0 A \qquad (4)$$

Fig. 5 – Plot of $(\alpha h\nu)^2$ vs $(h\nu)$

where 'C' is the capacitance, 'd' is the thickness of the sample, 'ε_0' is the permittivity of free space, and 'A' is the area of the sample. The dielectric constant with frequency for various temperatures is shown in Fig. 6. The curve reveals that the dielectric constant decreases with increase in frequency and then reaches almost a constant value in the high frequency region [16]. This also indicates that the value of the dielectric constant increases with an increase in the temperatures. The huge value of the dielectric constant at low frequencies can be attributed to the lower electrostatic binding strength, arising due to the space charge polarization near the grain boundary interfaces. Owing to the application of an electric field, the space charges are stimulated and dipole moments are produced and are called space-charge polarization. This apart, these dipole moments are rotated by the field applied ensuing in rotation polarization which also contributes to the high values.
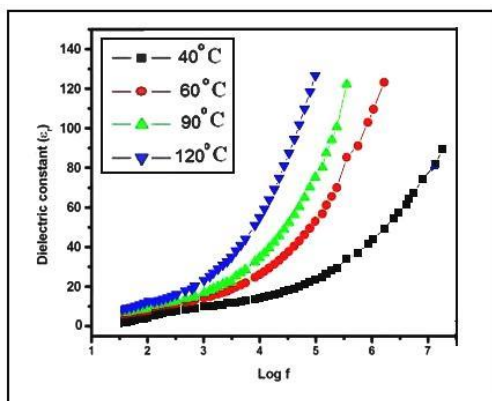

Fig. 6 – Dielectric constant of $BaTiO_3$ nanoparticles

Whenever there is an increase in the temperature, more dipoles are produced and the value increases [17]. Fig. 7 shows the variation of dielectric loss with respect to the frequency for various temperatures. These curves show that the dielectric loss is dependent on the frequency of the applied field, comparable to that of the dielectric constant. The dielectric loss decreases with an increase in the frequency at almost all temperatures, but appears to attain saturation in the higher frequency range at all the temperatures [18, 19].
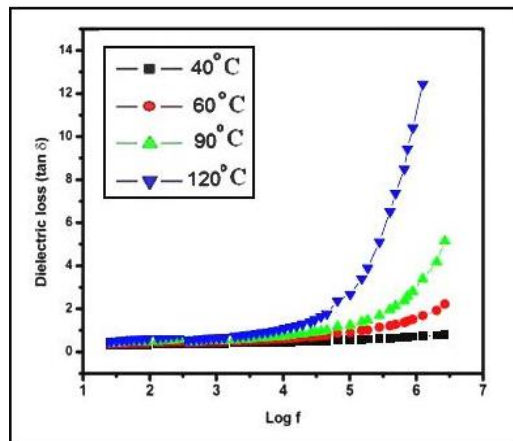

Fig. 7 – Dielectric loss of $BaTiO_3$ nanoparticles

4. AC ELECTRICAL CONDUCTIVITY STUDIES

Electrical measurements were taken in the frequency range 20 Hz to 1 MHz using HIOKI 3532-50 LCR HITESTER. A chromel-Alumel thermocouple was employed to record the sample temperature. The temperature dependent AC electrical conductivity study was carried out. The temperature dependent AC conductivity of the $BaTiO_3$ nanoparticles is shown in Fig. 8. It is observed that the conductivity (σ_{ac}) increases with an increase in the temperature and frequency. Traps which are present in the $BaTiO_3$ nanoparticles may be filled by excitation at low temperature and may be emptied by raising the temperature upon thermal activation. Upon thermal activation the mobility of charge carriers increases and it is possible that they adopt a hopping mechanism to cross the potential barrier and hence produce enhanced current.
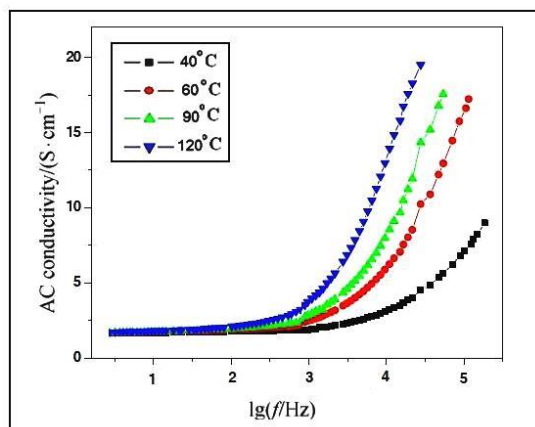

Fig. 8 – Variation of conductivity with log frequency

5. CONCLUSION

$BaTiO_3$ nanoparticles were prepared by solvothermal method. Their structural properties were investigated by XRD analysis. The average crystallite size of $BaTiO_3$ nanoparticles was calculated from the X-ray diffraction (XRD) pattern and found to be 22 nm. The scanning electron microscopy (SEM) analysis showed that the nanoparticles agglomerated forming spherical-shaped particles. The TEM results revealed that the particle size was measured in the range of 25 to 30 nm.

The optical properties were studied by the UV-Visible spectrum. The band gap value was found to be 3.40 eV. The dielectric constant and the dielectric loss of the $BaTiO_3$ nanoparticles were calculated for different frequencies and temperatures. The AC electrical conductivity was found to increase with an increase in the temperature and the frequency.

REFERENCES

1. D. Hennings, M. Klee, R. Waser, *Adv. Mater.* **3**, 334 (1991).
2. L.E. Cross, *Am. Ceram. Soc. Bull.* **63**, 586 (1984).
3. I.I. Naumov, L. Bellaiche, H. Fu, *Nature* **432**, 737 (2004).
4. H.C. Du, S. Wohlrab, M. Weiß, S. Kaskel, *J. Mater. Chem.* **17**, 4605 (2007).
5. P. Duran, D. Gutierrez, J. Tartaj, C. Moure, *Ceram. Int.* **28**, 283 (2002).
6. P.R. Arya, P. Jha, A.K. Ganguli, *J. Mater. Chem.* **13**, 415 (2003).
7. D.H. Yoon, B.I. Lee, *J. Ceram. Process. Res.* **3**, 41 (2002).
8. S. Bhattacharya, R. Tummalla, *J. Mater. Sci. Mater. Electron.* **11**, 253 (2000).
9. B. Cui, P.F. Yu, J. Tian, H.L. Guo, Z.G. Chang, *Mat. Sci. Eng. A* **454-455**, 667 (2006).
10. B. Cui, P.F. Yu, J. Tian, Z.G. Chang, *Mat. Sci. Eng. B* **133**, 205 (2006).
11. M. Viviani, M.T. Buscaglia, A. Testino, V. Buscaglia, P. Bowen, P. Nanni, *J. Eur. Ceram. Soc.* **23**, 1383 (2003).
12. M.Z.-C. Hu, G.A. Miller, E.A. Payzant, C.J. Rawn, *J. Mater. Sci.* **35**, 2927 (2000).
13. I.J. Clark, T. Takeuchi, N. Ohtori, D.C. Sinclair, *J. Mater. Chem.* **9**, 83 (1999).
14. S. Wada, H. Chikamori, T. Noma, T. Suzuki, *J. Mater. Sci.* **19**, 245 (2000).
15. Y. Kobayashi, A. Nishikata, T. Tanase, M. Konno, *J. Sol-Gel Sci. Technol.* **29**, 49 (2004).
16. S. Suresh, C. Arunseshan, *Appl. Nanosci.* **4**, 179 (2014).
17. Sagadevan Suresh, *Appl. Nanosci.* **4**, 325 (2014).
18. S. Suresh, *Int. J. Phys. Sci.* **8** No 21, 1121 (2013).
19. S. Suresh, *Int. J. Phys. Sci.* **9** No 17, 380 (2014).